5296 *Chem. Mater.* **2010,** *22,* 5296–5305
DOI:10.1021/cm101448a

CHEMISTRY OF MATERIALS
Article

# Synthesis and Optical Properties of Amorphous $Si_3N_{4-x}P_x$ Dielectrics and Complementary Insights from *ab Initio* Structural Simulations

J. B. Tice,[†] V. R. D'Costa,[‡] Gordon Grzybowski,[†] A. V. G. Chizmeshya,[†] J. Tolle,[†] J. Menendez,[‡] and J. Kouvetakis*,[†]

[†]*Department of Chemistry and Biochemistry, and* [‡]*Department of Physics, Arizona State University, Tempe, Arizona 85287*

*Received May 24, 2010. Revised Manuscript Received July 18, 2010*

Applications that require tuning of the properties of amorphous $Si_3N_4$ currently make use of non-stoichiometric silicon oxynitrides or silicon nitrides. In this study compositional tuning is employed to produce a new family of amorphous dielectrics with near stoichiometric $Si_3N_{4-x}P_x$ ($x \sim 0-1$) compositions and adjustable optical response. Air stable and thermally robust materials are deposited at 650−700 °C on Si wafers with a growth rates as high as 0.2 $\mu$m/min via CVD reactions of $P(SiH_3)_3$ with $NH_3$. An alternative route involving $P(SiH_3)_3/N(SiH_3)_3$ mixtures with ammonia was also explored and found to yield comparable materials. Precise control of the reactant fluxes produces alloys in which the $PSi_3$ molecular core of the precursor is likely incorporated intact into the covalent nitride network, leading to an assemblage of corner-shared $SiN_4$ and $SiN_3P$ tetrahedra containing residual N−H bonds. The optical properties of the resultant materials have been studied by spectroscopic ellipsometry, which indicated that the incorporation of P systematically decreases the band gap while increasing the refractive index. Density-functional theory simulations were used to reconcile the molecular geometry of the precursors with local bonding in the solids and predict that the incorporated $PSi_3$ cores adopt a planar geometry for low P contents (up to $x = 0.5$) and become slightly puckered as P increases to $x = 1$. This implies that the more rigid $Si_3N$ units initially induce a planarization in their softer $Si_3P$ counterparts, leading to hexagonal-type ground-state structures with slightly lower symmetry than that of the $\beta$-$Si_3N_4$ prototype. The simulations of the band-structure for $Si_3N_{3.5}P_{0.5}$ and $Si_3N_3P$ confirm the decreasing trend observed in the optical band gap as the P content is increased.

## I. Introduction

Alternatives to silicon dioxide ($SiO_2$) and silicon nitride ($Si_3N_4$), the traditional dielectric and passivation materials in semiconductor devices, have been the subject of intense research for the past two decades.[1] Of particular interest are alloy compounds whose properties can be tuned via compositional adjustments. These include materials such as silicon oxynitride ($SiO_xN_y$), with a refractive index that varies smoothly between that of $SiO_2$ (1.45) and $Si_3N_4$ (2.0) as the material's band gap decreases from 8 eV ($SiO_2$) to 4.5 eV ($Si_3N_4$) (refs 2 and 3). Even lower band gaps may be needed for future applications. For example, Er-doped $Si_3N_4$ has attracted attention as a possible route to the development of Si-compatible lasers at 1.55 $\mu$m. It has been found that an excess amount of Si (so-called silicon rich nitrides—SRN) lowers the band gap of the matrix and enhances its absorption coefficient, leading to higher Er excitation cross sections.[4] Unfortunately, excess Si also shortens the Er emission lifetime, which reduces the Er emission efficiency.[4] It thus appears that this technological approach would benefit from the ability to lower the band gap of the matrix independently of the Si concentration. Moreover, a band gap lower than that of $Si_3N_4$ would greatly improve the potential for electrical excitation of the Er ions. The resulting higher index of refraction would also facilitate the design of photonic structures and antireflection coatings.

In this work, we report the synthesis and optical characterization of $Si_3N_4$-related materials with these desired properties. The essence of our approach is the substitution of N atoms by isoelectronic P atoms, leading to a new family of amorphous $Si_3N_{4-x}P_x$ alloys with constant Si fraction in which the band gap decreases as a function of the P composition $x$. In addition to possible laser applications, the new $Si_3N_{4-x}P_x$ alloys may be of interest in other areas of semiconductor technology—such as passivation of III−V semiconductor surfaces—in which conventional silicon nitride finds widespread applications.[5,6]

*To whom correspondence should be addressed.

(1) Wilk, G. D.; Wallace, R. M.; Anthony, J. M. *J. Appl. Phys.* **2001**, *89*, 5243.
(2) Agnihotri, O. P.; Jain, S. C.; Poortmans, J.; Szlufcik, J.; Beaucarne, G.; Nijs, J.; Mertens, R. *Semicond. Sci. Technol.* **2000**, *15*, R29.
(3) Rebib, F.; Tomasella, E.; Gaston, J. P.; Eypert, C.; Cellier, J.; Jacquet, M. Journal of Physics; Conference Series 100; 2008; p 082033.
(4) Yerci, S.; Li, R.; Kucheyev, S. O.; Buuren, T. v.; Basu, S. N.; Negro, L. D. *Appl. Phys. Lett.* **2009**, *95*, 031107.
(5) Sah, R. E.; Rinner, F.; Baumann, H.; Kiefer, R.; Mikulla, M.; Weimann, G.; Dammann, M. *J. Electrochem. Soc.* **2003**, *150*, F129.
(6) Chou, Y. C.; Lai, R.; Li, G. P.; Jun, H.; Nam, P.; Grundbacher, R.; Kim, H. K.; Ra, Y.; Biedenbender, M.; Ahlers, E.; Barsky, M.; Oki, A.; Streit, D. *Electron Device Lett., IEEE* **2003**, *24*, 7.


Published on Web 08/16/2010

The synthetic concept adopted here to produce Si−P−N materials is based on reactions of $NH_3$ with a specially designed $P(SiH_3)_3$ precursor, which incorporates the P atom in a trigonal bonding configuration, as desired for substituting N by P in the classic $Si_3N_4$ alpha ($\alpha$) or beta ($\beta$) structures. Due to its high reactivity and unique internal bonding structure, the $(SiH_3)_3P$ is particularly well suited for low-temperature chemical vapor deposition (CVD) of the desired metastable compounds. It is routinely obtained in semiconductor-grade purity as a volatile colorless liquid, inherently devoid of carbon or halogen ligands which typically incorporate as deleterious impurities. While our synthetic scheme is based on the complete elimination of $H_2$ from $P(SiH_3)_3/NH_3$, we find that, under the low-temperature conditions required for the formation of the metastable structures and compositions, small amounts of H are inevitably incorporated, leading to hydrogenated $Si_3N_{4-x}P_x$ films in which the absence of long-range order produces an amorphous state. Nevertheless, the intrinsic covalent bonding controls the short-range structure, which should be indistinguishable from that of a corresponding bulk crystalline phase at the nanoscale. This is the well-known behavior in pure $Si_3N_4$, where the stoichiometry simultaneously accommodates the tetrahedral coordination of Si and the trigonal planar coordination of N, as in the case of the classic silylamine $N(SiH_3)_3$. We note that low-temperature reactions of the latter compound in ammonia are known to produce amorphous *a*-$Si_3N_4$. This raises intriguing questions about the possibility of structural inheritance when the N is replaced by P. In this regard, the corresponding stoichiometric $Si_3P_4$ compound has been predicted theoretically[7] to adopt defect-zinc blende structures as a ground state, in which the Si atoms remain tetrahedral while the $PSi_3$ units are puckered in analogy with the trigonal pyramidal core found in the $P(SiH_3)_3$ molecule.

In the present work, we use high-level *ab initio* simulations to explore the polymorphism in $Si_3N_{4-x}P_x$ alloys containing exclusively tetrahedral Si and diagonal $SiN_3$ and $PSi_3$ and bridging cores, particularly in the range of P compositions of $x < 1$ explored experimentally. A key finding is that the $PSi_3$ units are predicted to deviate from trigonal planar geometry as the P content increases, and the structural influence of the stiffer $NSi_3$ units diminishes. This leads to hexagonal-type ground-state structures with slightly lower symmetry than that of the $\beta$-$Si_3N_4$ prototype. Over this compositional range, our simulations of the band-structure confirm the decreasing trend observed in the optical band gap (e.g., via ellipsometry) as the P content is increased in the deposited materials. Our calculations also corroborate that full substitution of N by P leads to cubic and pseudocubic ground state structures.

## II. Results and Discussion

**(a) Synthesis.** The synthesis of hydrogenated amorphous films was achieved by reactions of varying proportions of $NH_3$ and $P(SiH_3)_3$ intermixed with high purity nitrogen gas. The $P(SiH_3)_3$ compound is produced as a colorless liquid with a vapor pressure of 18 Torr at 23 °C via a new and straightforward route in near quantitative yields and large scale amounts,[8] making it a viable reagent for exploratory and ultimately commercial synthesis of new materials incorporating $Si_3P$ building blocks. The depositions of $Si_3N_{4-x}P_x$ were conducted in a horizontal cold-wall reactor comprised of a cylindrical quartz chamber which is fitted with a cooling jacket that is maintained at 25−35 °C via recirculation of ethylene glycol through a refrigerated bath. The system is pumped down to a nominal base pressure of $10^{-9}$ Torr using a high-capacity turbo pump, and it is equipped with a load lock maintained at $10^{-8}$ Torr, allowing insertion of the substrates into the reactor without breaking vacuum. The substrates are placed on a graphite susceptor, inductively heated by an RF generator, and their temperature is measured with a single-color optical pyrometer. Prior to deposition, the high-density graphite block is thoroughly outgassed at 1100 °C under ultrahigh vacuum and then exposed to a flow of $SiH_4$ at 800 °C. The latter process creates a protective SiC layer, which prevents contamination of the samples from carbon and any other impurities potentially desorbing from the susceptor. A burn off furnace operating at 900 °C is fitted to the exhaust manifold of the reactor to pyrolyze unreacted gases and prevent release of harmful byproducts. Calibrated mass flow controllers were used to adjust the proportions of all reactants species and carrier gases in order to attain the desired film stoichiometry.

In a typical growth experiment, the Si(100) substrates with the native oxide intact were first degreased in a methanol ultrasonic bath, dried in a flow of $N_2$, and then inserted into the reactor and pumped to base pressure. The ammonia was then admitted into the reactor, a pressure of 50 Torr was immediately established using an automatic throttle valve, and the temperature was raised to 900 °C. The substrates were heated for 30 min under these conditions, and the temperature was then lowered to ~700 °C. An appropriate amount of the $P(SiH_3)_3$ compound, diluted with ultrahigh purity (UHP) $N_2$ at 10% by volume, was subsequently introduced and allowed to react on the Si surface at 650−700 °C to produce films at typical growth rates of 50−200 nm/min, yielding films possessing a smooth/shiny surface and a yellow-green-blue coloration typical of thin nitride layers. The film thicknesses ranged from 300 nm to 2.5 $\mu$m, as determined by Rutherford backscattering spectrometry (RBS) and corroborated by ellipsometry measurements. RBS at 2 MeV was also used to measure the Si and P concentrations while a resonance spectrum at 3.72 MeV was used to obtain the nitrogen content (see Figure 1). The corresponding oxygen and carbon resonance spectra indicated only background levels of these impurities in the bulk layer. In all cases, as shown in Figure 2, the relative concentration ([N] + [P])/[Si] remains close to the value $^4/_3$ expected for substitutional replacement of N by P. Finally, the H content was

(7) Huang, M.; Feng, Y. P.; Lim, A. T. L.; Zheng, J. C. *Phys. Rev. B* **2004**, *69*, 54112.

(8) Tice, J. B.; Chizmeshya, A. V. G.; Tolle, J.; D' Costa, V. R.; Menendez, J.; Kouvetakis, J. *Dalton Trans.* **2010**, *39*, 4551.

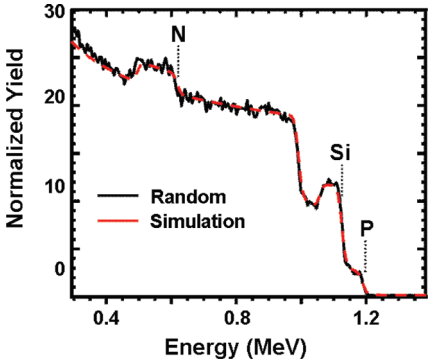


**Figure 1.** RBS spectrum of a $Si_{0.41}P_{0.09}N_{0.42}H_{0.08}$ film grown on Si(100). The red line represents the simulated fit of the above composition. Annealing at 900 °C reduces the H content to below the detection limit of 1%.

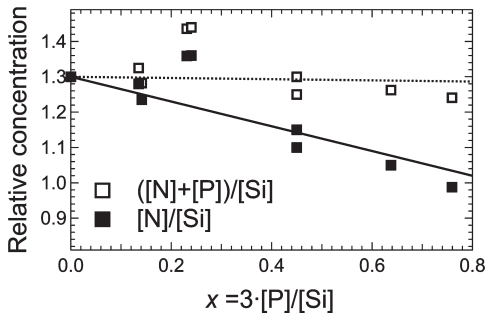


**Figure 2.** Relative concentrations of P, N, and Si in $Si_3N_{4-x}P_x/H$ films. The solid and dotted lines are fits to the data assuming that, for $x = 0$, [N]/[Si] = 1.30, as found for nominal $Si_3N_4/H$ films. The slope of the solid line is $-0.35 \pm 0.06$, and the slope of the dotted line is $-0.01 \pm 0.06$. Both values are in agreement with the expected slopes of $-1/3$ and zero, respectively.

measured by an elastic recoil detection (ERD) spectrum recorded at 2.8 MeV using a polymer target with a known H content as a reference. The combined atomic percentage of the Si, P, and N elements was ~92%, with the remaining 8% accounted for by hydrogen, which, as we discuss later in the IR analysis section, is bonded to the nitrogen atoms in the structural network. We note that all materials are not only thermally robust but also remarkably stable in air. This is consistent with the formation of highly resilient N−H bonds in favor of the much more reactive Si−H and P−H analogues. Accordingly, the N−H content, as we show below, is reduced significantly by thermal annealing.

The P concentration of the as deposited films was varied from 2 to 14% of the total Si−P−N content ($0.14 \leq x \leq 1$) by adjusting the amount of $P(SiH_3)_3$ in the reaction mixture to produce alloys with the general formula $Si_3N_{4-x}P_x$. In these experiments, we observe that the higher fluxes of $P(SiH_3)_3$, namely lower $NH_3/P(SiH_3)_3$ ratios, produce films with enhanced P content, ultimately leading to the upper limit of $x = 1$. The latter corresponds to a composition $Si_3N_3P$ that contains a P/Si ratio of $1/3$ identical to that of the precursor. In this case, we envision that the formation of the nitride solid proceeds according to the idealized reaction

$$P(SiH_3)_3 + 3NH_3 \rightarrow Si_3N_3P + 9H_2$$

As the flux of $P(SiH_3)_3$ is gradually reduced, we speculate that the reaction rate of the $NH_3$ molecules with the $SiH_3$ groups of the compound increases due to the presence of ammonia in large excess. This leads to a more complex range of decomposition channels, potentially yielding $-SiH_2-NH_2$ intermediates as well as $PH(SiH_3)_2$, $PH_2(SiH_3)$, and $PH_3$ derivatives of the starting material. The $-SiH_2-NH_2$ species then spontaneously condense films of silicon nitride-like materials, while the comparatively more stable phosphine analogues are incorporated at a significantly slower rate, ultimately leading to nitrogen-rich $Si_3N_{4-x}P_x$ alloys ($x < 1$). It is worth noting that the unimolecular decomposition of $P(SiH_3)_3$ diluted in $N_2$ at $T \sim 700$ °C and $P \sim 50$ Torr deposits Si/P films with a nominal stoichiometry of $Si_{0.80}P_{0.20}$, as determined by RBS. This composition is close to $Si_3P$ ($Si_{0.75}P_{0.25}$), indicating that the molecular cores of the compound are largely incorporated intact under these conditions. Accordingly, the addition of $NH_3$ at a certain critical threshold level promotes the reaction shown above, leading to the stoichiometric product $Si_3N_3P$. Increasing the ammonia flux above this level produces alloys with P concentrations in the range $x = 0.14-2.00$, as indicated earlier.

It is worth noting that in these reactions the growth rate increased in proportion to the P concentration in the final product, with typical rates of 200 nm/min for $Si_{0.43}N_{0.43}P_{0.14}$ and 40 nm/min for $Si_{0.43}N_{0.55}P_{0.02}$. The higher rates are attributed to the increased concentration of the highly reactive $P(SiH_3)_3$ in the mixture. To further investigate this effect, we conducted control experiments in which equimolar amounts of $P(SiH_3)_3$ and $N(SiH_3)_3$ (of the N analogue of the P compound) were reacted in an ammonia ambient similar to that employed in the reaction that produced $Si_{0.43}N_{0.43}P_{0.14}$ above. This produced films with composition $Si_{0.43}N_{0.47}P_{0.10}$ at a nominal rate of 100 nm/min, indicating that the introduction of the $N(SiH_3)_3$ reduced the activity of the much more reactive $P(SiH_3)_3$. Furthermore, we found that lowering the reaction temperature of $N(SiH_3)_3/P(SiH_3)_3$ to 600 °C yielded films with the same 10% P composition but at a much lower rate of 60−70 nm/min. These results suggest that $P(SiH_3)_3$ is in fact the limiting reagent due to its higher reactivity toward $NH_3$ and suggest that a suitable $P(SiH_3)_3/N(SiH_3)_3$ ratio (considerably less than 1:1) could also be found to yield a $Si_{0.43}N_{0.50}P_{0.07}$ ($Si_3N_{3.5}P_{0.5}$) compound. As we describe below, the latter composition is of particular interest because it can be assembled in principle using an equal number of $NSi_3$ and $PSi_3$ units, furnished by the corresponding silyl compounds, linked together with N provided by the ammonia to form an ordered lattice (see below). The $N(SiH_3)_3$ species employed in the above depositions was freshly prepared following literature routes and was thoroughly purified by fractional distillation. Finally, it is worth noting that the films produced under these conditions also contained ~8% H which was reduced to levels below 1% (the limit of the RBS measurement) by annealing the samples *in situ* at 900 °C under a flow of $NH_3$ at 50 Torr pressure. Remarkably, the $Si_{0.43}N_{0.47}P_{0.10}$ film stoichiometry remains unchanged.

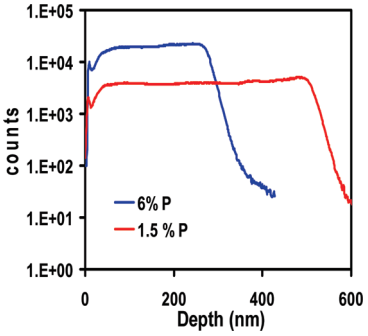


**Figure 3.** SIMS phosphorus profiles for two $Si_3N_{4-x}P_x$ films with RBS concentrations of 6 and ~1.5% P, respectively. The ratio of the ion count obtained from this data is ~4.5, which is close to the expected RBS value of ~4. The SIMS ion count is directly proportional to the atomic density in the sample, making the above comparison meaningful.

Additional characterizations of all samples (X-ray diffraction scans in $\theta - 2\theta$ mode) indicated that all films were essentially amorphous, as expected due to the relatively high hydrogen incorporation and the low temperature of deposition. Secondary ion mass spectrometry (SIMS) confirmed the presence of the Si, N, and P constituents for all samples across the compositional range and revealed uniform concentration profiles through the entire film thickness. The SIMS data were also used to corroborate the RBS phosphorus contents, particularly for low levels such as ~2−4%. In this case, since the absolute SIMS values could not be determined due to lack of suitable standards, we used ratios of the P signals and showed that they were identical with corresponding ratios of RBS compositions. An example is shown in Figure 3 for samples with RBS phosphorus contents of 1.5 and 6%, exhibiting a SIMS signal ratio of ~1:4, as expected. This approach is applicable here, since the scattering matrices are very similar due to the low P concentrations in the various samples considered.

The optical properties (see below) of the $Si_3N_{4-x}P_x$ alloys were quantified using a reference $Si_3N_4$ material which was specifically produced as part of this study following virtually identical synthesis protocols as for the P containing alloys. The reference $Si_3N_4$ materials were deposited *via* interactions of $NH_3$ and $(SiH_3)_3N$ as transparent and highly uniform layers on silicon substrates at 750 °C and a 50 Torr ammonia ambient. The samples were characterized for composition and crystallinity by XRD, RBS, and SIMS, and the results collectively indicated that the layers were amorphous and possessed a nominal composition of $Si_{0.40}N_{0.52}H_{0.08}$. These compositions were used to generate the $x = 0$ data point in Figure 2. It is important to note that the 8% hydrogen content in this material is nearly identical to that (7−9%) measured in the ternary alloys, allowing for a direct comparison between the two systems on an equal footing, as discussed below in the optical section of the paper.

**(b) Theoretical Simulations of $Si_3N_{4-x}P_x$ Structural Models.** We next considered possible crystalline structures for the Si−P−N films synthesized in our experiments. By simple comparative inference, nitrogen rich compositions ($x \sim 0$) might be expected to possess crystal structures similar to those of the well-known hexagonal $\beta$-$Si_3N_4$ phase in which the $SiN_4$ units adopt nearly ideal tetrahedral conformations and the $NSi_3$ units are completely trigonal-planar. This geometry is conferred, by structural inheritance, from the $N(SiH_3)_3$ molecule in which $\angle$Si−N−Si ~ 120°.[9] Accordingly, the $\beta$-$Si_3N_4$ prototype structure may not represent the best candidate for the phosphorus-rich $Si_3P_4$ compositions ($x \sim 4$), which are expected to contain irregular $SiP_4$ tetrahedra and trigonal pyramidal $PSi_3$ units, consistent with those observed in the $P(SiH_3)_3$ molecule ($\angle$Si−P−Si ~ 95°).[10] This is corroborated by recent theoretically studies of hypothetical $Si_3P_4$ solids, which conclude that a pseudocubic defect zinc-blende structure, in which one set of face-centered Si atoms is removed, is energetically preferred over the prototype $\beta$-$Si_3N_4$ structure.[7,11] To our knowledge, stoichiometric pure crystalline phases of $Si_3P_4$ have not yet been reported experimentally, and even more exotic low-energy structures may still exist. The apparent dichotomy in the structural chemistry of nitrogen- and phosphorus-based analogues, particularly with respect to the local bonding geometry around the N/P atoms, suggests that $Si_3N_{4-x}P_x$ alloys may exhibit a range of more complex structures than represented by hexagonal and cubic prototypes of their known $Si_3N_4$ and hypothetical $Si_3P_4$ end members, respectively.

To elucidate the crystal chemistry and ultimately predict the structural and electronic properties of the representative compositions $x = 0.5$ (7 atom % P) and $x = 1$ (14 atom % P), we undertook a brief series of first principles calculations based on density functional theory (DFT). All calculations were performed using the VASP code at the GGA level using PAW pseudopotentials.[12] The electronic structure is described using a plane-wave basis with an energy cutoff of 500 eV and a reciprocal space quadrature grid whose density and symmetry is judiciously chosen to ensure convergence of ground state properties. Typically, $5 \times 5 \times 5$ Monkorst−Pack grids were used for cubic and tetragonal systems while $4 \times 4 \times 8$ Γ-centered grids were used for hexagonal systems possessing small $c/a$ ratios. With these settings, the atomic forces and cell stress were converged to 0.01 eV/A and 0.01 GPa, respectively.

In order to investigate how the structures of the $PSi_3$ molecular cores are modified by their incorporation into the solid phase, we also calculated the equilibrium structure of the $P(SiH_3)_3$ precursor by placing it into a large (slightly orthorhombic) supercell with edge lengths ~12 Å and optimizing only atomic coordinates. Using the above pseudopotentials, energy cutoffs, and a single $k$-point for Brillouin-zone sampling, the static equilibrium Si−P bond length and a Si−P−Si bond angle were found to

(9) Hedberg, K. *J. Am. Chem. Soc.* **1955**, *77*, 6491.
(10) Blake, A. J.; Ebsworth, E. A. V.; Henderson, S. G. D. *Acta Crystallogr.* **1991**, *C47*, 486.
(11) Xu, M.; Wang, S.; Yin, G.; Chen, L.; Jia, Y. *Opt. Express* **2006**, *14*, 710.
(12) Kresse, G.; Furthmuller, J. *Comput. Mater. Sci.* **1996**, *6*, 15. Kresse, G.; Hafner, J. *Phys. Rev. B* **1993**, *47*, 558. Kresse, G.; Furthmuller, J. J. *Phys. Rev. B* **1996**, *54*, 11.

be 2.26 Å and 95.2°, respectively, in excellent agreement with the corresponding observed values of 2.25 Å and 95.5°.[10] Similar agreement is also found for the trisilylamine molecule $N(SiH_3)_3$, for which the calculated N−Si bond length and Si−N−Si bond angle are 1.75 Å and 120°, respectively, with corresponding observed values of 1.74 Å and 120°.[9]

An exhaustive survey of the structural trends in $Si_3N_{4-x}P_x$ alloys on the basis of all known $Si_3N_4$ phases as well as the various proposed $Si_3P_4$ structures is well beyond the scope of our paper. Our primary interest here is in the nitrogen-rich compositions accessed in our synthesis experiments, namely up to a maximum P incorporation of $x = 1$ (e.g., $Si_3PN_3$). Accordingly, we limit our simulations to only four relevant candidate structures: (i) the prototype "$\beta$-$Si_3N_4$" structure containing planar $Si_3N$ or $Si_3P$ units, as shown schematically in Figure 4a and b, (ii) a variant of the "$\beta$-$Si_3N_4$" denoted by $\delta$-$Si_3X_4$ ($x$ = N and P) in which the planar constraint is lifted, allowing the N or P atoms to move off plane, as shown in Figure 4c for the representative $Si_3N_3P$ phase, (iii) a cubic defect-zinc blende structure, $c$-$Si_3X_4$, which explicitly incorporates trigonal-pyramidal $Si_3N/Si_3P$ units, and (iv) a tetragonal modification of $c$-$Si_3X_4$, designated as $t$-$Si_3X_4$, which accommodates a partial planarization of the pyramidal $XSi_3$ units, as shown in Figure 4d. We note that the c-phase analogue corresponds to a structure in which $c = a$. While the cubic and tetragonal prototypes are based on the results of previous theoretical studies on the $Si_3P_4$ system, the $\delta$-$Si_3X_4$ derivative of the $\beta$-$Si_3N_4$ prototype is explored here for the first time. The $\delta$-$Si_3X_4$ modification was suggested by our initial optimizations of the $Si_3PN_3$ and $Si_3P_{0.5}N_{3.5}$ alloys in the $\beta$-$Si_3N_4$ structure, which identified a local minimum in which all $Si_3P$ units remained trigonal-planar. However, this configuration was found to be dynamically unstable with respect to small vertical (out-of-plane) displacements of the trigonal centered P or N, suggesting that additional energy lowering should be achieved by allowing this degree of freedom. As we shall demonstrate below (Table 1), this is borne out by explicit calculations.

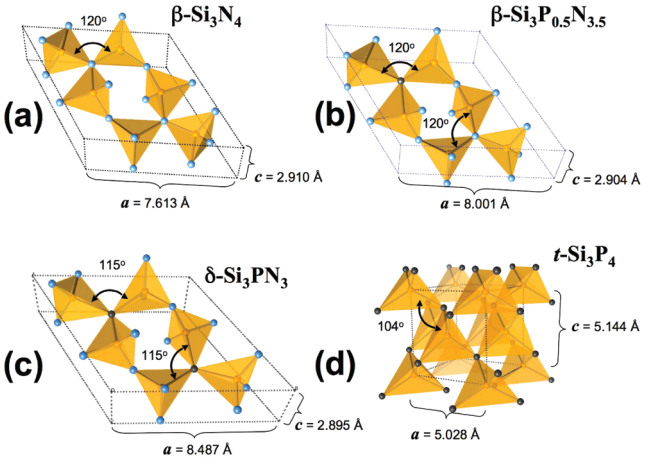


**Figure 4.** Ground state structures of the $Si_3N_{4-x}P_x$ systems with $x = 0, 1, 2, 4$. The nitrogen rich $Si_3N_4$ and $Si_3P_{0.5}N_{3.5}$ condense in the classical $\beta$-type structures shown in parts a and b, respectively. The puckered variant presented in part c is adopted by the $Si_3N_3P$ with a P content of $x = 1$, while further increase in P produces the tetragonal polytype of the $Si_3P_4$ derivative shown in part d. The cubic polytype of the latter phase is essentially identical to the slightly tetragonal shown here. Lattice parameters correspond to the equilibrium values listed in Table 1, and the Si−P−Si and Si−N−Si angles (in degrees) are superimposed upon the structures.

The structural trends across the $Si_3N_{4-x}P_x$ alloys can also be understood from a polyhedral perspective in which the structures of $Si_3N_4$ and $Si_3P_4$ can be viewed as being composed entirely of corner-shared $SiN_4$ and $SiP_4$ tetrahedra, respectively. The incorporation of $PSi_3$ units in place of $NSi_3$ in the $Si_3N_4$ lattice creates $SiPN_3$ tetrahedra in proportion to the amount of P introduced. Accordingly, a lattice comprised entirely of $SiPN_3$ tetrahedra yields the composition $Si_3PN_3$, corresponding to a $\sim x = 1$. On the other hand, an equal mixture of fully networked $SiN_4$ and $SiPN_3$ tetrahedra corresponds to the $Si_3P_{0.5}N_{3.5}$ alloy with a ~7 atom % P content, as shown in Figure 5. Also shown in Figure 5 is the equilibrium molecular structure of the $P(SiH_3)_3$ and $N(SiH_3)_3$ precursors, with arrows indicating the placement of the cores within the crystalline unit cell containing two $Si_3N_{3.5}P_{0.5}$ formula units. As can be seen from the figure, each

**Table 1. Static Equilibrium Crystal Structures and Energies of $Si_3N_4$, $Si_3P_{0.5}P_{3.5}$, $Si_3PN_3$, and $Si_3P_4$ in the Four Candidate Lattice Structures $c$-$Si_3X_4$, $t$-$Si_3X_4$, $\beta$-$Si_3N_4$, and $\delta$-$Si_3X_4$[a]**

| | system | symmetry | $a$ (Å) | $c$ (Å) | angles (deg) | $V$/atom (Å) | $E$/atom (eV) | $\Delta E$/atom (meV) |
|---|---|---|---|---|---|---|---|---|
| $x = 0$ | $c$-$Si_3N_4$ | cubic | 4.1054 | | 90°, 90°, 90° | 9.885 | −7.9799 | 244 |
| | $t$-$Si_3N_4$ | tetragonal | 4.0632 | 4.1721 | 90°, 90°, 90° | 9.840 | −7.9622 | 262 |
| | **$\beta$-$Si_3N_4$** | **hexagonal** | **7.6132** (*7.595*) | **2.9104** (*2.902*) | **90°, 90°, 120°** | **10.434** | **-8.2239** | **0** |
| | $\delta$-$Si_3N_4$ | hexagonal | 7.6132 | 2.9104 | 90°, 90°, 120° | 10.434 | −8.2239 | 0 |
| $x = 1$ | $c$-$Si_3P_{0.5}N_{3.5}$ | ~cubic | 4.2200 | | 91.8°, 88.2°, 88.2° | 10.736 | −7.5673 | 160 |
| | $t$-$Si_3P_{0.5}N_{3.5}$ | ~tetragonal | 4.2088 | 4.2834 | 92.1°, 88.1°, 88.3° | 10.816 | −7.5833 | 144 |
| | **$\beta$-$Si_3P_{0.5}N_{3.5}$** | **hexagonal** | **8.0007** | **2.9037** | **90°, 90°, 120°** | **11.496** | **-7.7268** | **0** |
| | $\delta$-$Si_3P_{0.5}N_{3.5}$ | hexagonal | 7.9666 | 2.9062 | 90°, 90°, 120° | 11.408 | −7.7210 | 6 |
| $x = 3$ | $c$-$Si_3PN_3$ | ~cubic | 4.3250 | | 93.5°, 86.5°, 86.5° | 11.490 | −7.1612 | 203 |
| | $t$-$Si_3PN_3$ | ~tetragonal | 4.3182 | 4.4373 | 94.1°, 85.9°, 86.4° | 11.733 | −7.2158 | 149 |
| | $\beta$-$Si_3PN_3$ | hexagonal | 8.4383 | 2.8938 | 90°, 90°, i20° | 12.744 | −7.3301 | 34 |
| | **$\delta$-$Si_3PN_3$** | **hexagonal** | **8.4867** | **2.8948** | **90°, 90°, 120°** | **12.895** | **-7.3645** | **0** |
| $x = 4$ | $c$-$Si_3P_4$ | cubic | 5.0456 | | 90°, 90°, 90° | 18.350 | −5.3543 | 83 |
| | **$t$-$Si_3P_4$** | **tetragonal** | **5.0280** | **5.1441** | **90°, 90°, 90°** | **18.578** | **-5.4372** | **0** |
| | $\beta$-$Si_3P_4$ | hexagonal | 9.7523 | 3.6842 | 90°, 90°, 120° | 21.674 | −5.3102 | 127 |
| | $\delta$-$Si_3P_4$ | hexagonal | 9.7697 | 3.6588 | 90°, 90°, 120° | 21.602 | −5.3281 | 109 |

[a] For each composition, $\Delta E$/atom represents the energy difference between a given phase and the ground state structure, in meV.

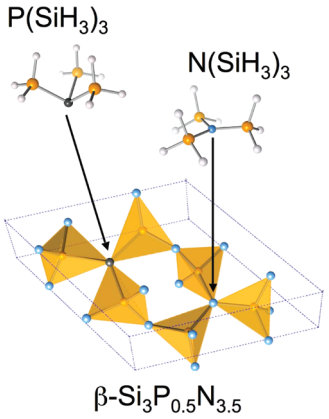


**Figure 5.** Structural representation of the $Si_3P_{0.5}N_{3.5}$, including the optimized molecular structures of $P(SiH_3)_3$ and $N(SiH_3)_3$ obtained from DFT calculations using PAW-GGA methods. The arrows denote the placement of the "$PSi_3$" and "$NSi_3$" cores within the unit cell. Legend: silicon (yellow), phosphorus (black), nitrogen (blue), and hydrogen (white).

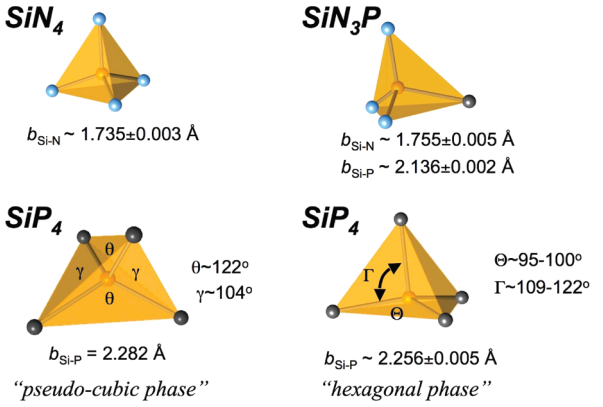


**Figure 6.** $SiN_4$, $SiPN_3$, and $SiP_4$ tetrahedral building blocks contained in the $Si_3N_{4-x}P_x$ alloy structures. Bond length and bond angle distributions are given in angstroms and degrees.

P center is surrounded by three Si sites in a slightly trigonal−pyramidal geometry, as expected, while the nitrogen bonding closely follows the trigonal planar conformation found in the well-known $\beta$-$Si_3N_4$ structure and in the trisilyl amine compound.

The structures and shapes of the basic $SiN_4$, $SiP_4$, and $SiN_3P$ building blocks for the $Si_3N_{4-x}P_x$ ($x$ = 0, 1, 2, 4) systems are shown in Figure 6. In the pure nitride phase, the $SiN_4$ units (top left) exhibit a narrow range of bond lengths at ~1.735 ± 0.003 Å and N−Si−N angles approaching the near ideal value 109.5° ± 2. By contrast, the $SiP_4$ units (bottom left) of pseudocubic $Si_3P_4$ are significantly distorted, with the internal P−Si−P angles ranging from 94 to 122°. Remarkably, all Si−P bond lengths remain identical at 2.282 Å, which is slightly longer than the 2.26 Å quoted above for the $P(SiH_3)_3$ precursor. The $SiP_4$ units in the higher energy hexagonal structure exhibit a very narrow distribution of bond lengths at ~2.256 ± 0.005 Å, but these tetrahedra are nevertheless deformed, with the P atom shifted significantly toward the " basal face" of the unit, as shown at the bottom right of Figure 6. This anomalous asymmetry is likely linked to the metastability of the hexagonal phase relative to the pseudocubic ground state. The intermediate $SiN_3P$ tetrahedra exhibit Si−N and Si−P bond lengths that are slightly longer and shorter, respectively, than those found in the pure phases, while the bond angles seem to depend on the P stoichiometry. For $x$ = 0.5 (7% P), the N−Si−P angles range from 96 to 110° degrees, while, for $x$ = 1 (14% P), the corresponding range is 105 to 117°. These are systematically below and above the ideal tetrahedral values, respectively.

Our principal computational results are summarized in Table 1, which lists the static lattice equilibrium lattice parameters, volumes, and energies of the $Si_3N_4$, $Si_3N_{0.5}P_{3.5}$, $Si_3N_3P$, and $Si_3P_4$ compositions corresponding to the four candidate lattice structures described above ($\beta$-$Si_3N_4$, $\delta$-$Si_3X_4$, $t$-$Si_3X_4$, and $c$-$Si_3X_4$). In each case, the lowest energy polymorph is designated by bold font, while static energy differences (in meV) are listed for the remaining phases. Note that the corresponding static equilibrium structures adopted by the alloys are those shown in Figure 4. For the pure nitride composition, our calculations predict the $\beta$-$Si_3N_4$ phase as the ground state structure, and the corresponding lattice parameters are in excellent agreement with the experimental values given in parentheses. We note that the lower symmetry $\delta$-$Si_3N_4$ phase reverts back to the $\beta$-type structure, indicating that the out-of-the plane displacement of the nitrogen atoms of the $NSi_3$ group is unfavorable, as expected. This energy penalty for deforming the $NSi_3$ planar conformation is even more severe in the cubic ($c$-$Si_3X_4$) or tetragonal ($t$-$Si_3X_4$) phases whose equilibrium structures possess energies far above that of the $\beta$-$Si_3N_4$ ground state (~250 meV/atom). In contrast to the case of $Si_3N_4$, the energy difference between the planar $\beta$- and puckered $\delta$-variant of $Si_3N_{3.5}P_{0.5}$ is exceedingly small (6 meV), indicating that the rigid and planar $NSi_3$ units slightly overwhelm the "puckering" tendency of the $PSi_3$ units. For the $Si_3P_{0.5}N_{3.5}$ composition, the optimized cubic ($c$-$Si_3X_4$) or tetragonal ($t$-$Si_3X_4$) phases represent the high-energy structures (~150 meV/atom). Although this is also true in the more P-rich $Si_3PN_3$ composition, the corresponding $\Delta E$'s are slightly larger (150−200 meV/atom) for these pseudocubic and -tetragonal structures. Here, however, the complete absence of $NSi_3$ units allows the $PSi_3$ cores to lower their energy by "puckering", such that the $\delta$-$Si_3PN_3$ phase becomes more favored by $\Delta E \sim +34$ meV/atom than the $\beta$-$Si_3PN_3$ form, which contains planar $PSi_3$ units. Finally, the pure $Si_3P_4$ composition condenses in the $c$-$Si_3X_4$ and $t$-$Si_3X_4$ structures, with the tetragonal variant being favored over the cubic by about 80 meV/atom. We note that the $t$-$Si_3P_4$ phase possesses a ground state energy 127 meV/atom lower than that of $\beta$-$Si_3P_4$, indicating that planar $Si_3P$ is not compatible with this latter structure. This is consistent with earlier DFT-GGA calculations on the $Si_3P_4$ system,[9] which reported $\Delta E$(c-$\beta$) ~175 meV.

Collectively our results indicate that the ground state structures of the $Si_3N_{4-x}P_x$ alloys arise from a subtle competition between the tendency of $Si_3N$ units to remain planar and the tendency of the corresponding $Si_3P$ units to "pucker", as expected. Accordingly, as P is gradually incorporated into the $Si_3N_4$ lattice, the more rigid $Si_3N$

units initially induce a planarization in their softer $Si_3P$ counterparts. This is found in the $Si_3P_{0.5}N_{3.5}$ alloy structure (7% P), where both the Si−N−Si and Si−P−Si angles are 120°. As the phosphorus content is further increased beyond $x = 0.5$, the influence of the $Si_3N$ units decreases, culminating in $Si_3N_3P$, where all $Si_3P$ units adopt a pyramidal-trigonal symmetry with the Si−P−Si angles being 115°. In general, therefore, as the P content increases, the Si−P−Si angle within the $Si_3N_{4-x}P_x$ system progresses from a value of 120° in the pure nitride ($x = 0$) to 104° in the pure phosphide ($x = 4$), tending toward the intrinsic free-molecular value of 95° observed in the structure of the precursor. As mentioned earlier, the perfect planarity of the $Si_3N$ units within the above structures can be traced to that of the $N(SiH_3)_3$ molecule, which is used to produce the reference $Si_3N_4$ films discussed in the Experimental Section. The close similarity of the bond lengths and angles between $P(SiH_3)_3$ ($b_{Si-P}$ = 2.26 Å, ∠Si−P−Si = 95.2°) and $Si_3P_4$ ($b_{Si-P}$ = 2.29 Å, ∠Si−P−Si = 103.7°) suggests that the latter might be accessible via reactions of this molecule and a suitable source of P, such as $PH_3$, according to the reaction

$$P(SiH_3)_3 + 3PH_3 \rightarrow Si_3P_4 + 9H_2$$

In an analogous fashion, the $Si_3P_{0.5}N_{3.5}$ composition could be accessed by reactions of suitably tuned mixtures of $P(SiH_3)_3$ and $N(SiH_3)_3$ with appropriate amounts of ammonia, as implied by Figure 5.

Another intriguing finding of the simulations studies is that Vegard's law appears to hold across the compositional range considered in our study in spite of the dichotomy in cubic and hexagonal symmetries in the P-rich and N-rich structures. This can be readily verified by taking the cube root of the equilibrium volume for each stable phase to obtain a characteristic length scale, $L$. For the 7% P alloy $Si_3P_{0.5}N_{3.5}$, $V_{VEG}$ = 11.45 Å$^3$, yielding $L$ = 2.25 Å while the corresponding calculated value from Table A1 is 2.26 Å. Similar consideration for the 14% P $Si_3PN_3$ phase ($V_{VEG}$ = 12.47 Å$^3$) yields $L$ = 2.32 Å, which corresponds closely to the calculated value $L$ = 2.34 Å for $V_{CALC}$ = 12.90 Å$^3$. We note that Vegard's Law does not appear to apply if all the above compositions are restricted to the $\beta$-structure.

**(c) Optical Properties.** An infrared variable angle spectroscopic ellipsometer (J. A. Woollam, Co.) was used to acquire data at room temperature in the energy range between 0.04 and 0.65 eV. The measurements were performed at three angles of incidence: 55°, 65°, and 75°. The samples were described as a three-layer system consisting of a Si substrate, a $Si_3N_{4-x}P_x$ film layer, and a surface layer. The surface layer was modeled as a thin film consisting of 50% $Si_3N_{4-x}P_x$ and 50% voids in the Bruggeman approximation. UV−visible spectroscopic ellipsometry measurements were carried out at room temperature using a variable angle spectroscopic ellipsometer (J. A. Woollam, Co.) with a computer-controlled compensator. The ellipsometric angles Ψ and Δ were determined at an angle of incidence of 65°. The dielectric function was extracted from the data using the procedure described in ref 13.

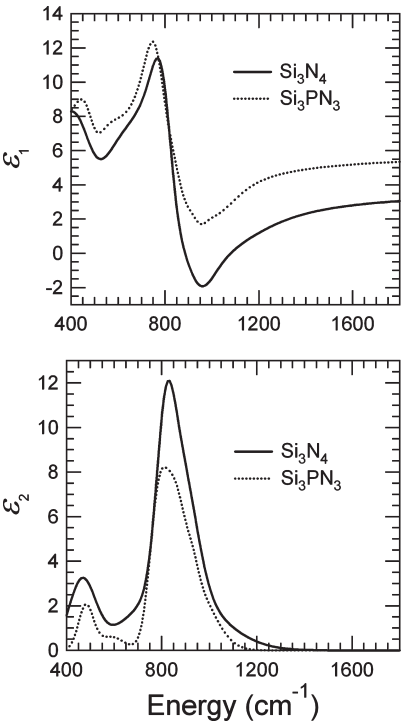


**Figure 7.** Complex infrared dielectric function of a $Si_3PN_3$ film and a $Si_3N_4$ film.

*Infrared Optical Constants.* Figure 7 shows the infrared dielectric function obtained for an $Si_3N_{3.02}P_{0.98}$ film compared with a reference $Si_3N_4$ sample grown under a similar approach. The two functions are remarkably similar, except for a reduction in magnitude as N is replaced by P. They are also very similar to published infrared optical constants for amorphous silicon nitride.[14−16] The imaginary part $\varepsilon_2$ of the dielectric function shows three peaks at 471 cm$^{-1}$, 644 cm$^{-1}$, and 825 cm$^{-1}$ in $Si_3N_4$ and slightly shifted frequencies in $Si_3N_{3-x}P_x$. Weaker features observed at 1130 cm$^{-1}$ and 3350 cm$^{-1}$ are consistent with the presence of N−H bonds and will not be discussed any further. It is customary in the literature to analyze vibrational spectra in terms of the absorption coefficient α. For the broad peaks found in the infrared absorption of amorphous materials, this may cause some confusion regarding mode frequencies, since α-maxima and $\varepsilon_2$-maxima do not appear at the same frequency. For example, the 471 cm$^{-1}$, 644 cm$^{-1}$, and 825 cm$^{-1}$ peaks in $\varepsilon_2$ translate into peaks at 485, 654, and 911 cm$^{-1}$ in α, in good agreement with published values based on infrared transmission measurements.[14,15] We prefer to use the frequencies extracted from $\varepsilon_2$ maxima because they are directly related to the mode vibrational frequencies. The use of transmission

(13) D'Costa, V. R.; Cook, C. S.; Birdwell, A. G.; Littler, C. L.; Canonico, M.; Zollner, S.; Kouvetakis, J.; Menendez, J. *Phys. Rev. B* **2006**, *73*, 125207.
(14) Tsu, D. V.; Lucovsky, G.; Mantini, M. J. *Phys. Rev. B* **1986**, *33*, 7069.
(15) Yin, Z.; Smith, F. W. *Phys. Rev. B* **1990**, *42*, 3666.
(16) Klanjšek Gunde, M.; Maček, M. *Phys. Status Solidi* (*A*) **2001**, *183*, 439. Klanjšek Gunde, M. *Appl. Spectrosc.* **1992**, *46*, 365.

spectra to study the vibrational structures may also lead to artificial thickness dependencies of the mode frequencies.[18] The mode frequencies reported here for the reference $Si_3N_4$ film are in excellent agreement with those measured by Klanjšek Gunde and Maček,[16] which are also based on an analysis of $\varepsilon_2$.

The infrared vibrational spectrum of $Si_3N_4$ has been discussed in the literature in terms of local modes of the $Si_3N$ unit, assuming that the amorphous phase preserves the planar geometry with three Si neighbors surrounding an N atom.[14,17] Recent *ab initio* studies of $Si_3N_4$ by Giacomazzi and Umari confirm this geometry.[18] Within this model, the main peak at 825 $cm^{-1}$ is assigned to an asymmetric in-plane bond-stretching vibration. The line shape of this peak is clearly asymmetric, requiring at least two symmetric oscillators in a model fit. It has been speculated that these oscillators correspond to vibrations of 3-fold and 2-fold coordinate N, respectively.[16] This interpretation, however, appears to be inconsistent with *ab initio* studies which find frequencies well above 1000 $cm^{-1}$ for doubly bonded N.[18] The same calculations reproduce very nicely the asymmetric line shape seen in Figure 2 based solely on the stretching vibrations of triple-bonded N. There is a continuum of such modes between 600 $cm^{-1}$ and 1250 $cm^{-1}$, giving rise to the broad main infrared peak. Thus, we believe that a fit of the feature with two or more oscillators provides a useful parametrization of the data but does not necessarily correspond to groups of modes with physically distinct characteristics.

The second most intense feature in Figure 7 appears at 471 $cm^{-1}$ for $Si_3N_4$. It has been assigned by Lucovsky et al. to a totally symmetric breathing movement of the three Si atoms relative to the N atom in the $Si_3N$ unit.[17] The infrared activity of this mode is supposed to derive from the presence of second-neighbor hydrogen atoms. Giacomazzi and Umari, on the other hand, find that this peak corresponds to out-of-plane displacements of the N atoms, which they denote as "rocking" motions.[18] Such out-of-plane vibrations were estimated by Lucovsky et al. to have lower frequencies around 300 $cm^{-1}$.

The weakest feature in Figure 7 is a peak at 644 $cm^{-1}$ that is also observed by Yin and Smith and assigned to vibrations of the $Si_3N$ bonding unit.[15] The *ab initio* calculations show two weaker peaks near this range,[18] but larger supercells may be needed to make a definitive assignment. A possible way to reconcile the detailed first principles calculation of Giacomazzi and Umari with Lucovsky's simplified analysis in terms of the $Si_3N$ unit would be to assign the 644 $cm^{-1}$ feature to the Si-breathing mode. It may be possible to confirm this assignment by carefully analyzing the mode eigenvectors from ref 18.

The interpretation of the *a*-$Si_3N_4$ vibrations in terms of local modes of the skeletal $Si_3N$ group provides a natural explanation for the observed infrared dielectric function in $Si_3N_{4-x}P_x$. Assuming the substitutional replacement of N by P, as in the theoretical simulations discussed above, modes with large eigenvector components on the central atom are likely to display a "two-mode" behavior consisting of nitrogen-like vibrations of the $Si_3N$ unit and phosphorus-like vibrations of the $Si_3P$ unit. Moreover, since our simulations predict that the unit structures stay planar for $x < 1$, the nitrogen-like vibrations should remain essentially intact upon P incorporation, except for second-neighbor force-constant changes. The major observable effect of the incorporation of P would then be a reduction in the intensity of the nitrogen-like modes due to the reduced number of $Si_3N$ units. This is in qualitative agreement with the experimental observation, except that the reduction in intensity is somewhat stronger than the $1 - x/4$ dependence predicted by simple bond counting. The $Si_3P$ group vibrations should occur at much lower frequencies due to the larger P mass, and their relative strength should be proportional to $x/(4 - x)$. This amounts to less than $^1/_4$ for our samples, but the actual strength may be even less if the effective charges are reduced in the case of $Si_3P$ due to the increased covalency of the bond. Thus, it is not surprising that we do not see any unequivocal indication of $Si_3P$ vibrations, which may occur near the low-energy limit of the dielectric function in Figure 7 and overlap with the low-energy $Si_3N$ vibrations.

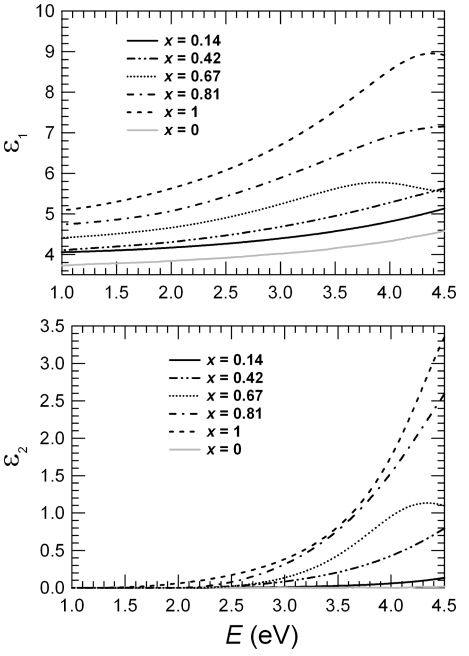


**Figure 8.** Complex dielectric function of $Si_3N_{4-x}P_x$ films and a reference $Si_3N_4$ sample.

*Visible−UV Optical Constants*. The visible−UV dielectric function extracted from the $Si_3N_{4-x}P_x$ films is shown in Figure 8. The magnitude of the real part of the dielectric function at low energies increases monotonically as a function of the P concentration $x$, indicating a refractive index increase. We fit this low-energy range with an expression of the form $\varepsilon_1(E) = \varepsilon_\infty + AE + BE^2$, where $A$ and $B$ are constants, and from these fits we obtain the electronic dielectric constant $\varepsilon_\infty$, which is plotted in Figure 9 as a function of the P concentration $x$. The value $\varepsilon_\infty = 3.7$ for

(17) Lucovsky, G.; Yang, J.; Chao, S. S.; Tyler, J. E.; Czubatyj, W. *Phys. Rev. B* **1983**, *28*, 3234.
(18) Giacomazzi, L.; Umari, P. *Phys. Rev. B* **2009**, *80*, 144201.

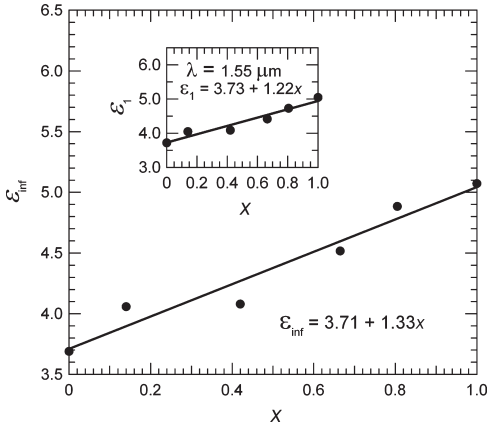


**Figure 9.** Dielectric function at optical frequencies $\varepsilon_\infty$ for $Si_3N_{4-x}P_x$ alloy films.

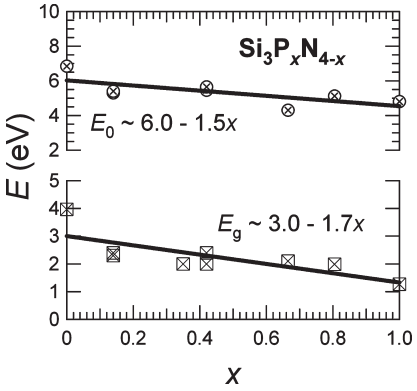


**Figure 10.** Compositional dependence of the $E_0$ and $E_g$ parameters in the Tauc−Lorentz model for $Si_3N_{4-x}P_x$.

$Si_3N_4$ is somewhat lower than the value $\varepsilon_\infty = 4.1$ obtained by Jellison and Modine.[19] (Notice that we use the standard definition for the electronic dielectric constant, so that our value of $\varepsilon_\infty$ corresponds to $\varepsilon_{1TL}(0)$ in Jellison and Modine's notation.) Our finding for the electronic dielectric constant is also in good agreement with the *ab initio* prediction $\varepsilon_\infty = 3.9$.[18] In Figure 9 we also show the real part of the dielectric constant at 1.55 $\mu$m, which should be useful for the design of photonic structures based on $S_3N_{4-x}P_x$ alloys.

The imaginary part of the dielectric function shows a monotonic red-shift with respect to $Si_3N_4$ as the P-fraction is increased. The overall energy dependence of the dielectric function is very well described by a single Tauc−Lorentz oscillator, as proposed by Jellison and Modine for $Si_3N_4$[19] and other amorphous materials. This model includes as adjustable parameters a band gap $E_g$, an average valence-conduction band separation $E_0$, an amplitude $A$, and a broadening $C$. The absorption is exactly zero below $E_g$. An extension of the model to include Urbach-tail absorption below $E_g$ was developed by Foldyna et al.,[20] but our ellipsometric measurements are not sensitive to the exponentially decreasing Urbach tails, so that we use the simpler Tauc−Lorenz model to analyze our data.

In Figure 10 we show the compositional dependence of the two energy parameters $E_g$ and $E_0$. The parameter $E_g$ for our $Si_3N_4$ films is found to be very sensitive to the growth method, ranging from $E_g = 3.5$ eV to $E_g = 4.5$ eV. For comparison, Jellison and Modine find $E_g = 4.50$ eV, whereas Bauer[21] finds a very similar value for $Si_3N_4$ grown by sputtering but much larger band gaps ~5.3 eV for samples grown by CVD. Given this strong sensitivity to the growth method, the band gap $E_g$ for $Si_3N_{4-x}P_x$ can only be compared among samples grown under the same conditions, including $Si_3N_4$. Such data have been fit with a linear dependence in Figure 10, but it is apparent that the data is also consistent with a discontinuous decrease of about 1 eV upon initial P incorporation, followed by a weaker decrease as the P concentration is increased. A smooth compositional dependence might be expected if a virtual-crystal approach is valid to describe the alloy electronic structure, whereas a discontinuous change should be observed if the incorporation of P leads to electronic levels deep within the band gap of $Si_3N_4$. The theoretical calculations discussed below do seem to support an interpretation of Figure 10 in terms of a large band gap decrease upon the initial P incorporation followed by a weaker compositional dependence.

The parameter $E_0$ is far more robust than $E_g$ in that it is not sensitive to the growth parameters. All of our $Si_3N_4$ samples, for example, yield $E_0 = 6.4$ eV, regardless of growth details. The compositional dependence of $E_0$ is also modeled as a simple linear dependence, and we find that the slope is similar to that found for the lowest band gap $E_g$, suggesting a more or less rigid closing of the band gap upon P incorporation. Since the fit parameters are close or beyond the range of our measurements, we have carried out a few experiments over an extended range up to 6.5 eV. In all cases, we find exactly the same fit parameters, indicating that the reduced measurement range up to 4.5 eV is sufficient to determine the parameters of the Tauc−Lorentz model used to analyze the data.

The strong variability of $E_g$ might cast some doubts on the physical significance of this parameter, particularly since the most important approximation of the Tauc−Lorentz model, as discussed above, is to neglect absorption below $E_g$. The Tauc−Lorenz−Urbach function used to extend the model[20] is significantly different from the simplified Tauc−Lorenz function near $E = E_g$, so that fits with this model might yield different values of $E_g$. However, such fits may require measurements over a larger dynamic range of absorption values than possible with ellipsometry. On the other hand, the *ab initio* calculations of Giacomazzi and Umari[18] suggest a physical basis for the variability of $E_g$. These authors find that double-bonded N defects and triple-bonded Si defects form localized electronic levels at the top of the valence band and the bottom of the conduction band, respectively. If the different growth methods lead to very different concentrations of such defects, this may provide an explanation for the fluctuations in $E_g$. The existence of band edge states associated with P may additionally contribute to these fluctuations in $Si_3P_xN_{4-x}$ alloys.

(19) Jellison, G. E., Jr.; Modine, F. A. *Appl. Phys. Lett.* **1996**, *69*, 371.
(20) Foldyna, M.; Postava, K.; Bouchala, J.; Pistora, J.; Yamaguchi, T. In *SPIE*; Jaromir, P. , et al., Eds.; 2004; p 301.
(21) Bauer, J. *Phys. Status Solidi* (*A*) **1977**, *39*, 411.

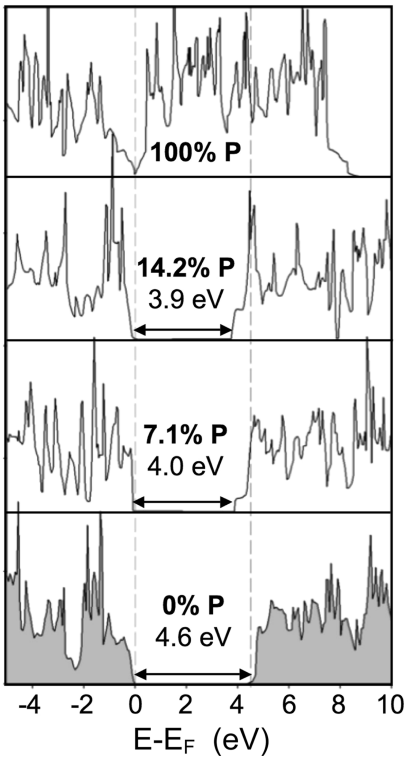


**Figure 11.** Density of states for $\beta$-$Si_3N_4$ (0% P), $\beta$-$Si_3P_{0.5}N_{3.5}$ (7% P), $\beta$-$Si_3PN_3$ (14% P), and $\beta$-$Si_3P_4$ (100% P), indicating that P incorporation leads to an abrupt change in band gap from a value of 4.6 eV in the pure nitride to ~4 eV. Note the band gap vanishes in the "non-ground-state" $\beta$-$Si_3P_4$ analogue.

Since our theoretical structure analysis of crystalline $Si_3P_xN_{4-x}$ phases described above yielded electronic structure as a byproduct of the calculations here, we plot the resulting density of states (DOS) for the $\beta$-$Si_3N_4$ (0% P), $\beta$-$Si_3P_{0.5}N_{3.5}$ (7% P), and $\beta$-$Si_3PN_3$ (14% P) in order to obtain a first estimate of the dependence of the band gap, $E_g$, on P concentration. As shown in Figure 11, the $E_g$ value in the pure nitride is predicted to be ~4.6 eV using the GGA prescription, which, as LDA, is known to underestimate experimental values. In fact, the experimental value for $\beta$-$Si_3N_4$ is $E_g = 5.5$ eV.[22] We find that P substitution into the lattice at the level of $x \sim 0.5-1$ leads to a band gap decrease of ~15%. Thus, the theoretical calculations reproduce semiquantitatively the observed compositional dependence of the band gap in our amorphous films, although the predicted decrease is substantially less than observed experimentally. While it is difficult to ascertain to what extent crystalline phase calculations can be used to make quantitative predictions about the amorphous phase optical properties, it is interesting to note that the calculations also appear to reproduce the nonlinear dependence of the band gap on P concentration suggested from the experimental data, namely a large decrease for small P concentrations, followed by a weaker dependence as the P concentration is further increased. Also shown in Figure 11 (top panel) is the DOS of the corresponding pure P analogue in the $\beta$-type isostructural $Si_3P_xN_{4-x}$ series, which nevertheless is *not* the cubic ground state structure identified in Figure 4. While the band gap in the $\beta$ structure is predicted to vanish, its value in the cubic phase was recently calculated to be ~0.8 eV.[11] Collectively, this suggests that the band gap in $Si_3P_xN_{4-x}$ alloys decreases from ~4−6 eV in the pure nitride to a value of 0−0.8 eV in the pure phosphide, depending on the local geometry of the $Si_3P$ units. In the case of amorphous materials containing non-negligible H content, the band gap is expected to follow a similar trend.

(22) Carson, R. D.; Schnatterly, S. E. *Phys. Rev. B* **1986**, *33*, 2432.

## III. Conclusion

We have described the growth and optical properties of $Si_3N_{4-x}P_x$, a new family of alloy dielectrics with a silicon-nitride-like structure. Our results indicate that it is possible to manipulate the optical properties while keeping the Si concentration constant. As expected, the incorporation of P lowers the band gap and increases the refractive index, providing a new tool to tailor the properties of this material for semiconductor applications. Theoretical calculations were used to follow the structural and energetic evolution of the $Si_3N_{4-x}P_x$ alloys, including their pure binary end members $Si_3N_4$ to $Si_3P_4$.

**Acknowledgment.** This work was supported by the U.S. Air Force under Contract DOD AFOSR FA9550-06-01-0442 (MURI program), by the U.S. Department of Energy under Contract DE-FG36-08GO18003, and by the National Science Foundation under Grant DMR-0907600.